

TiO₂-B/Ag Nanocomposite Wires Enhanced Electrochemical Performance for Li-ion Batteries

Jinlong Wang¹, Kaixin Song^{1,*}, Changqing Tong¹, Guanglei Tian², Jun Wu¹, Huifang Gao¹ and Junming Xu¹

¹College of electronic information and engineering, Hangzhou Dianzi University, 310018, Hangzhou

²College of Materials Science and Environment engineering, China Jiliang University, 310018, Hangzhou

Received: June 25, 2017, Accepted: September 18, 2017, Available online: September 25, 2017

Abstract: In this work, the pristine and Ag-composited TiO₂-Bronze (TiO₂-B) nanowires are successfully synthesized by hydrothermal method using anatase(P25) as titanium source. The SEM, TEM results reveal that the silver particles are well distributed on the TiO₂-B nanowires. Also, the TiO₂-B/Ag nanowires are dispersed very well, which demonstrate more Li-ion insertion/extraction hosts exposed to the electrolyte. Moreover, the electrochemical performance tests suggest that compared with the pristine TiO₂-B, the Ag-composited TiO₂-B (TiO₂-B/Ag) shows remarkably higher capacities (~286mAhg⁻¹, closing to the theoretical capacity) and superior rate capability. The reasons causing this performance difference are ascribed to the added silver particles, which could reduce the Li-ion diffusion length and improve the material electrical conductivity.

Keywords: Hydrothermal, TiO₂-B/Ag, Nanowires

1. INTRODUCTION

The tremendous consumption and increasing depletion of fossil fuel resources by traditional energy production, as well as the increased pollution they have caused, highlight the urgent demand for renewable energy [1–4]. Because of their superior properties such as high energy density, high power density, light weight, and long cycle stability et al., lithium ion batteries (LIBs) have been widely used as power sources in hybrid electric vehicles (HEVs) and electric vehicles (EVs) [5–7]. The graphite is extensively used as a commercial anode material for LIB. It will stores Li⁺ when to form LiC₆ with a flat voltage, V≈0.2V (vs. Li/Li⁺) through an intercalation process. However, a LiC₆ charged anode forms a passivating solid-electrolyte interphase (SEI) layer that consumes Li⁺ from the cathode. The SEI layer prevents uniform plating out of Li during charge. Moreover, in the process of fast charging and discharging, the dendrites forming on the anode may penetrate the separator and short-circuit the cell creating a severe fire hazard [8,9]. Compared to the commercial graphite anodes, Li₄Ti₅O₁₂ (LTO) exhibits a relatively high lithium insertion/extraction potential of 1.6V~1.7V (vs. Li/Li⁺), which avoided the SEI formation in

standard electrolyte solutions and suppresses lithium dendrite deposition on the surface of the anode. However, the low storage capacity of LTO (175mAh/g in theory) has prevented its widespread use [11-13].

Titanium dioxide is considered as one of the most promising anode materials for lithium ion batteries due to its abundant natural resources, non-toxicity and low cost [14]. Compared to anatase(P25), brookite and rutile, bronze crystalline titania (TiO₂-B) belongs to monoclinic system. 1986, Marchand et al firstly reported the synthesis of TiO₂-B by 500°C heat treatment to Hydrogenated titanic acid, which got from the K₂Ti₄O₉ ion exchange. TiO₆ octahedra in the TiO₂-B structure connect with each other by sharing the vertex and corner. In the direction of a, b and c, TiO₂-B has a more open space in that it is very suitable for Lithium ion intercalation/deintercalation [15]. In addition, TiO₂-B has a high reversible specific capacity, thermal stability and low volume expansion (<=4%) in the process of intercalation/deintercalation, which can effectively avoid the collapse of the electrode material because of the large change between the charge and discharge, significantly improved the material cycle performance and electrochemical stability.

Research shows that TiO₂-B is a pseudo-Faraday induced current process with pseudo-capacitance effect, while the implanta-

*To whom correspondence should be addressed: Email: kxsong@hdu.edu.cn
Phone: 13588198089

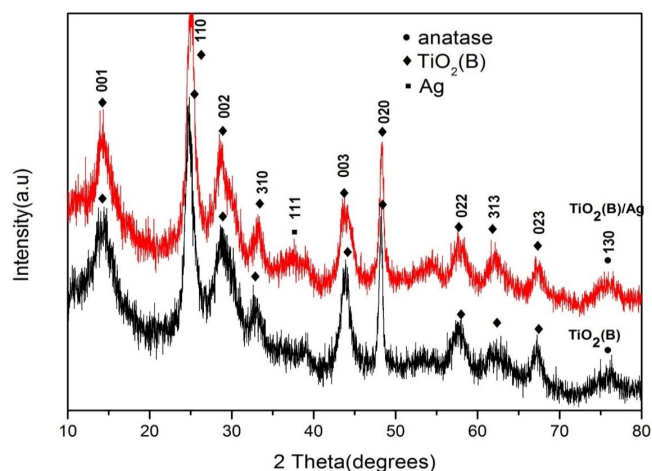


Figure 1. XRD patterns of $\text{TiO}_2\text{-B}$ and $\text{TiO}_2\text{-B/Ag}$ hybrid.

tion of anatase and rutile is a solid diffusion process, so $\text{TiO}_2\text{-B}$ can carry out rapid charge and discharge [16]. However, the low electric and ionic conductivities within $\text{TiO}_2\text{-B}$ limits its application to commercial lithium batteries. To overcome these issues, the current research mainly based on the material morphology and composite, such as synthesis nanoparticles, nanowires, nanosheets to improve the electrochemical properties of the material. At the same time, composites was compounded on the basis of the preparation of different morphology $\text{TiO}_2\text{-B}$ with the materials of good conductivity such as carbon, graphene and Cu to improve the synergistic effect of $\text{TiO}_2\text{-B}$ [17-19]. Some electrode material for lithium ion battery with good electrochemical performance were prepared. Specifically, hybridizing $\text{TiO}_2\text{-B}$ with carbonaceous materials (carbon nanotubes, graphene, etc.) has attracted a lot of attentions [22,23,24]. Among those carbonaceous materials, the two-dimensional (2D) graphene is commonly used because of its high conductivity, structural flexibility [20,21,23,25-27]. Zhang et al [28] synthesized $\text{NiO/TiO}_2\text{-B}$ nanocomposites by hydrothermal and precipitation method. The first charge and discharge capacity was 395mAh/g at 0.1C rate. Capacity retention was 96.2% after 50 cycles. The capacity retention rate was higher than that of pure $\text{TiO}_2\text{-B}$ which was 87.4%. Lan et al [29,30]. Prepared $\text{TiO}_2\text{-B/graphene}$ nanocomposites by one-step hydrothermal route, and the discharge capacity decreased from 205.3mAh/g to 189.4mAh/g when cycling from 4 to 300. The average decrease ratio of capacity during circulation is 0.026%. Zhang et al [31]. Synthesized Cu-doped $\text{TiO}_2\text{-B}$ nanowires by the microwave assisted hydrothermal method. The doped nanowires show a specific capacity of 186.8mAh/g at the 10C rate with capacity retention of 64.3% after 2000 cycles. Remarkably, our material exhibits a specific capacity of 150mAh/g at the 60C rate, substantiating its superior high rate capability for rechargeable lithium batteries.

To find a more effective doping species, herein we prepared $\text{TiO}_2\text{-B/Ag}$ nanowires composites by hydrothermal method. Next, we compared with the pure $\text{TiO}_2\text{-B}$ nanowires. The obtained nanocomposites could not only increase the capacity of $\text{TiO}_2\text{-B}$, but also display excellent cycling and rate performances as anode materials for LIBs.

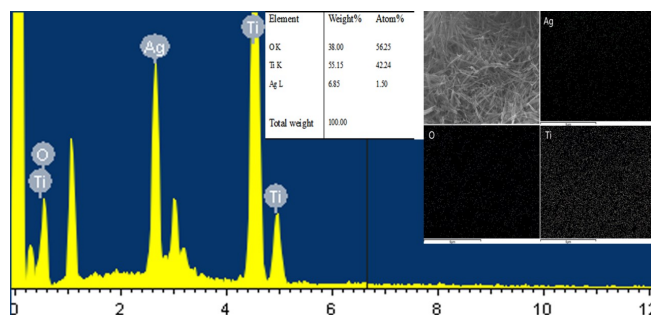


Figure 2. EDS and Mapping of $\text{TiO}_2\text{-B/Ag}$ hybrid

2. EXPERIMENTAL SECTION

2.1. Materials

P25, Silvernitrate (AgNO_3), sodium hydroxide (NaOH), hydrochloric acid (HCl), distilled water, and deionized water were used. All chemicals were used further purification.

2.2. Preparation of Nanowires of $\text{TiO}_2\text{-B/Ag}$ nanowire composites

Typically, 1.48g P25 into 40mL 10mol/L sodium hydroxide solution, stir for 2h and then add Silvernitrate to continue stirring for 2h, then transferred to 50mL hydrothermal reactor. And placed in oven at 180°C for 72h, then cool to room temperature and remove. The resulting product was washed three times with deionized water, centrifuged and filtered to add right amount of 0.1mol/L HCl. The mixed filtrate was stand for 24h after stirred for 30min. Rinse the solution to pH=7 using deionized water. The resulting white precipitate was dried in an oven at 70°C for 12h and then heat-treated in a tube furnace at 410°C (heating rate 5°C/min) for 2h to obtain an off-white powder product for subsequent Characterization and performance testing.

In contrast, pure $\text{TiO}_2\text{-B}$ samples without any composite materials were prepared by using P25 as raw material and the same preparation process.

2.3. Material Characterization

The room-temperature crystalline phase constituents were identified by powder X-ray diffraction (XRD) (RIGAKU/max 2550/PC, Rigaku Co, Tokyo, Japan) analysis with $\text{CuK}\alpha$ ($\lambda=1.54056\text{\AA}$) radiation at the voltage of 40kV and current of 30mA. The scanning rate was 10°min^{-1} in the 2θ range from 10 to 80°. The surface morphologies of the $\text{TiO}_2\text{-B}$ and $\text{TiO}_2\text{-B/Ag}$ hybrid nanomaterials were examined using a scanning electron microscope (SEM, Hitachi, Japan) and a transmission electron microscope (TEM, TecnaiF20). The samples for TEM measurement were prepared by dispersing the composite materials in ethanol and placing a drop of the clear solution onto a carbon-coated copper grid followed by drying. The Energy dispersive spectroscopy (EDX) and elemental mapping analyses were performed using a Ni grid (200 meshes) as the sample holder.

2.4. Electrochemical Measurements

For the electrochemical measurement of lithium-ion intercalation, the above samples were assembled into a half cell. The $\text{TiO}_2\text{-B}$

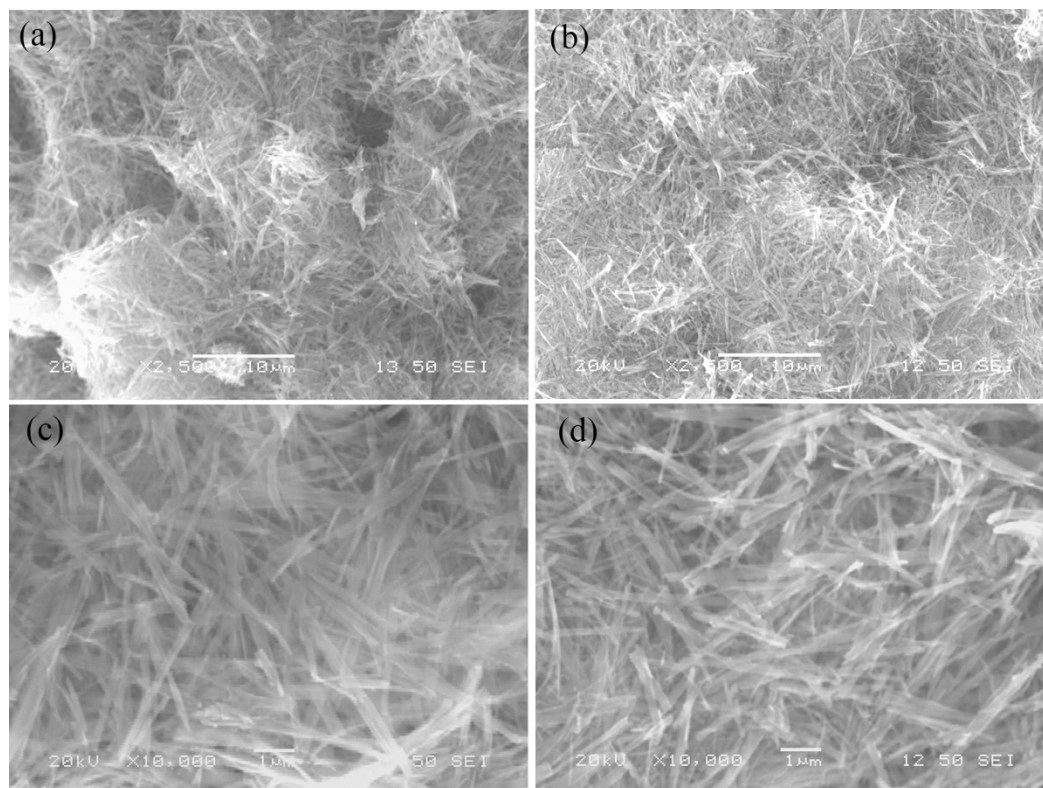


Figure 3. SEM images of two samples: low magnification of TiO₂-B (a), TiO₂-B/Ag(b),high magnification of TiO₂-B (c),TiO₂-B/Ag(d)

B and TiO₂-B/Ag were mixed with polyvinylidene fluoride (PVDF) binder and acetylene black carbon additive in a weight ratio of 70:15:15, respectively. The mixture was spread and pressed on copper foil circular flakes as working electrodes (WE), and dried at 120°C in vacuum for 12h. Lithium foils were used as the counter electrodes. The electrolyte was 1M LiPF₆ in a 1:1:1 (volumeratio) mixture of ethylene carbonate (EC), ethylene methylcarbonate (EMC) and dimethyl carbonate (DMC). The separator was Celgard2400 (America) micro-porous polypropylene membrane. The cells were assembled in a glove box filled with highly pure argon gas (O₂ and H₂O levels < 1ppm), and charge/discharge tests were performed in the voltage range of 1.0 to 3.0 V (Li⁺/Li) at different current densities on a Neware automatic batteries tester (Neware CT-3008, Shenzhen, China). Cyclic voltammetry (CV) and electrochemical impedance spectroscopy (EIS) were collected in the voltage range of 1.0 to 3.0V (Li⁺/Li) on electrochemistry workstation (CHI6608B).

3. RESULTS AND DISCUSSION

The XRD patterns of TiO₂-B and TiO₂-B/Ag are illustrated in Fig.1. It can be seen that the XRD patterns of the two samples obtained under the experimental conditions are basically the same. The characteristic peaks of Ag appear in the XRD patterns of the composites at 38°, but the other peak indicates that no other new phase produces, while the peak intensity and peak width are almost the same, indicating that the crystallinity of TiO₂-B has not been greatly affected by Ag composite. At the same time, at 77°there is a weak anatase characteristic peak, indicating that both samples have

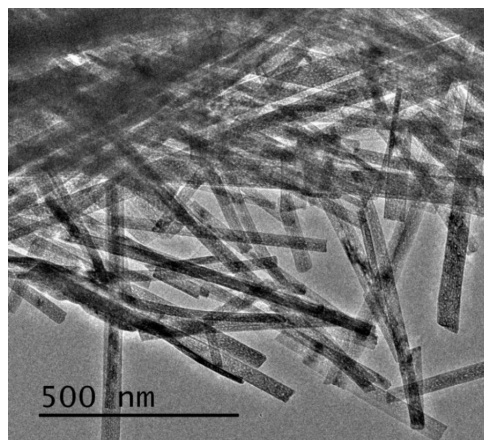


Figure 4. The TEM images of TiO₂-B/Ag nanocomposite tubes

a small amount of anatase phase produced.

In order to further determine the composition of the composite material, we use the energy dispersive spectroscopy (EDS) and element mapping to analyze the elements in the samples qualitatively and quantitatively. The spectrum of the TiO₂-B/Ag sample as Fig.2 show, which confirmed that Ag was successfully compound with TiO₂-B and distributed uniformly and continuously on TiO₂-B nanowires.

To observe the morphology of the TiO₂-B and TiO₂-B/Ag hybrid, the samples were measured by SEM and TEM. Fig.3 is a one-

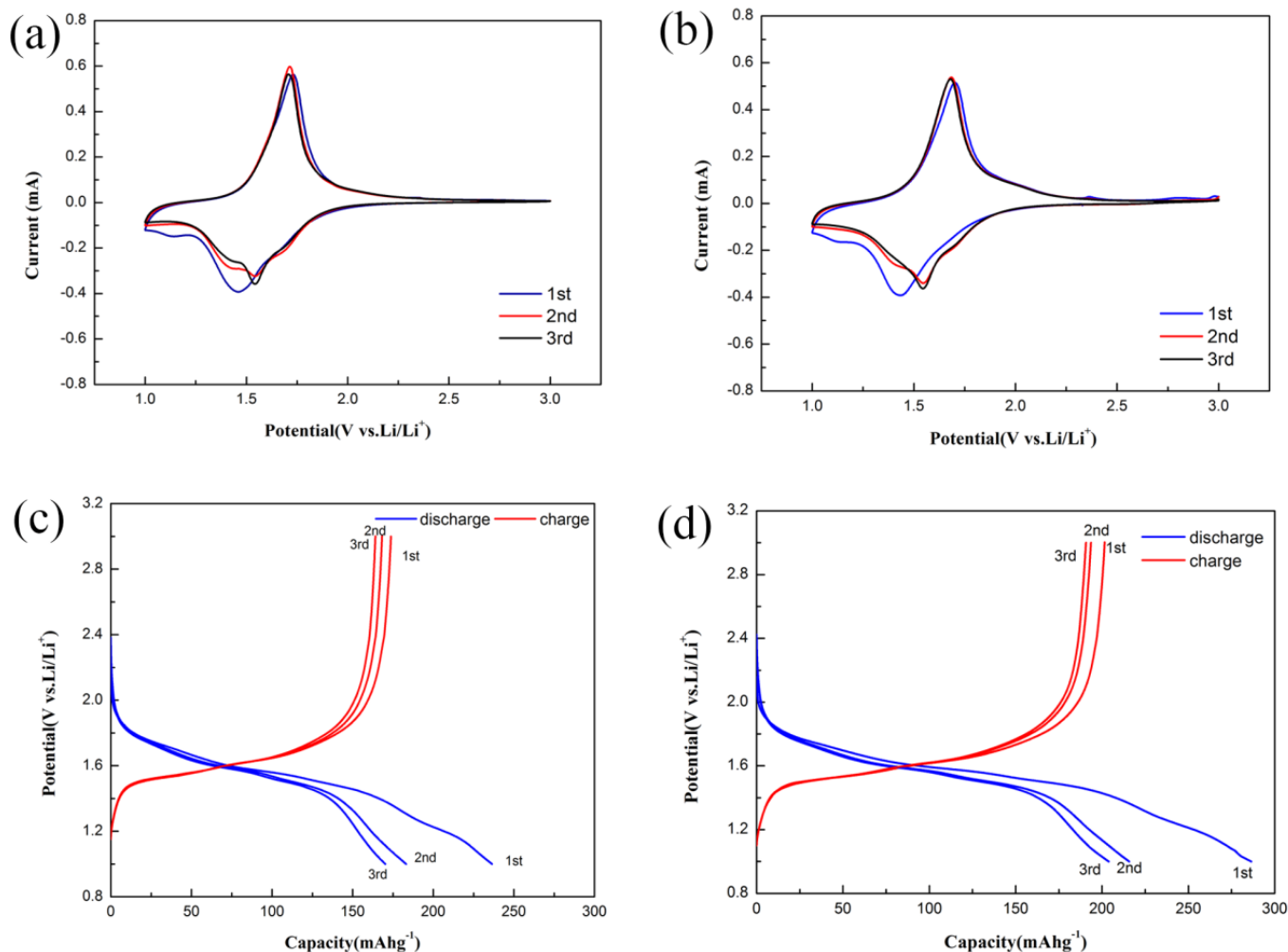


Figure 5. CV curves of the cell made of (a) $\text{TiO}_2\text{-B}$ and (b) $\text{TiO}_2\text{-B/Ag}$ hybrid at a scan rate of 0.5 mVs^{-1} ; Charge-discharge profiles of the cells made of (c) $\text{TiO}_2\text{-B}$ and (d) $\text{TiO}_2\text{-B/Ag}$ hybrid at a current density of 0.1 C .

dimensional bronze crystalline nano- $\text{TiO}_2\text{-B}$ and its composites with Ag low and high magnification of the scanning electron microscope, Fig.3a and b can be seen that at low magnification of the prepared $\text{TiO}_2\text{-B}$ and $\text{TiO}_2\text{-B/Ag}$ nanocomposites are linear, evenly distributed, while there is a slight reunion phenomenon. However, there was no significant difference in the morphology of the two samples, and it was found that the composited Ag did not have a significant effect on the morphology. Fig.3c and d for the sample at 10,000 times can clearly see the material of linear shape, uniform length.

Fig.4 shows TEM images of bronze crystalline titanium dioxide $\text{TiO}_2\text{-B/Ag}$ nanometer linear composites. It can be seen that $\text{TiO}_2\text{-B}$ exists in a linear morphology, the sample $\text{TiO}_2\text{-B/Ag}$ nanowires formation width evenly, width is about 45nm , 275nm to several micrometers in length, and there is no obvious agglomeration phenomenon, while high TEM no other morphology except $\text{TiO}_2\text{-B/Ag}$.

To evaluate the electrochemical properties of the two samples, CV was carried out at a scan rate of 0.5 mV/s between 1.0 from

3.0V . As depicted in Fig.5. The samples of $\text{TiO}_2\text{-B}$ and $\text{TiO}_2\text{-B/Ag}$ nanocomposite electrode materials were observed at 1.5V and 1.75V in the first scanning process from Fig.5a and b. At the same time, due to the influence of the SEI film, the second and the third charge and discharge cycle of the reduction peak occurred offset. Moreover, the two groups of samples were almost coincident with the reduction oxidation peak in the three times scanning, which indicated that the $\text{TiO}_2\text{-B/Ag}$ nanocomposite electrode had good electrochemical stability. Simultaneously, the structure of $\text{TiO}_2\text{-B/Ag}$ is stable in the process of lithium ion insertion and removal.

Fig.5c and d show the charge-discharge profiles of $\text{TiO}_2\text{-B}$ and $\text{TiO}_2\text{-B/Ag}$ nanocomposite electrode materials. It can be seen that the charging platform of the two sets of samples is about 1.5V , which corresponds to the reduction peak of the CV curves. Similarly, the discharge platform is about 1.75V , which corresponds to the oxidation peak of the CV curves. At the same time, the specific discharge capacity of $\text{TiO}_2\text{-B}$ and $\text{TiO}_2\text{-B/Ag}$ was 236.465mAh/g and 286.369mAh/g , respectively. The specific capacity of the composites was higher than that of pure $\text{TiO}_2\text{-B}$. Indicating that the

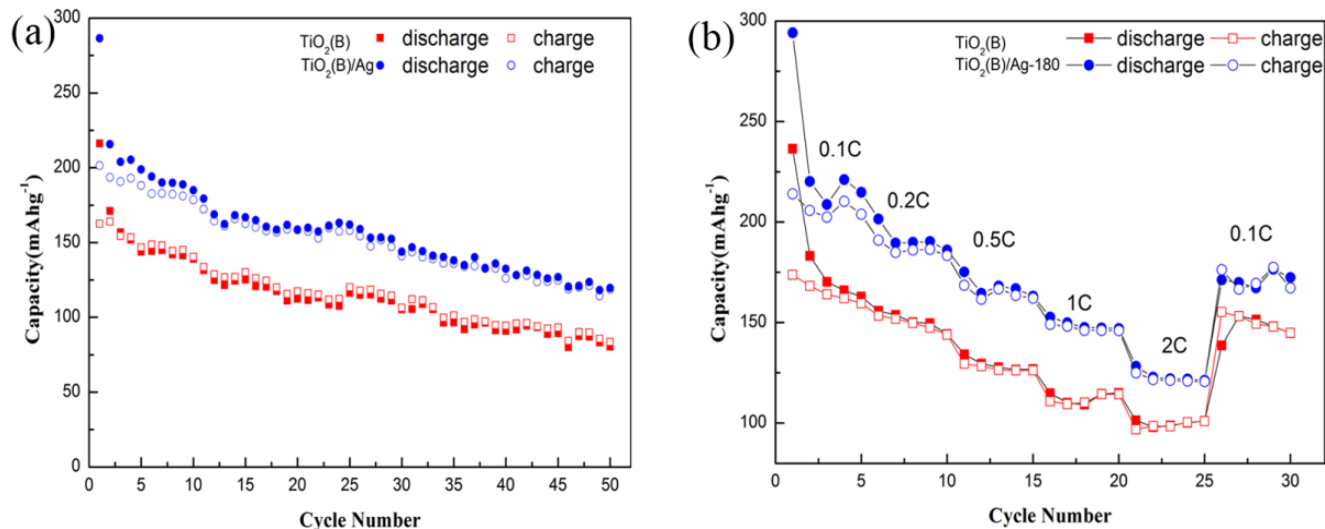


Figure 6. (a) cycling performances at a current density of 0.1C for TiO₂-B and TiO₂-B/Ag hybrid and (b) rate capabilities from 0.1 to 2C, respectively.

composite with Ag to enhance the first charge and discharge capacity of the material.

Fig.6a is a sample of pure TiO₂-B and sample TiO₂-B/Ag 50 charge and discharge cycle capacity chart. The composite discharge capacity is much higher than the non-composite materials. Ag composite can effectively enhance the electrochemical performance of TiO₂-Bnanowires.TiO₂-B/Ag rate of capacity loss of in the circulation process almost the same, in to 50 cycles. The discharge specific capacity ofTiO₂-B and TiO₂-B/Ag were 95.2mAh/g and 126.5mAh/g.

The rate capabilities of TiO₂-Band TiO₂-B/Ag hybrid were evaluated by charge-discharge at various current densities from 0.1 to 2C for every each 5cycles (Fig.6b). It clearly reveals that both of them exhibited excellent capacity retentions at each current density. The discharge capacity of the two sets of samples at the high current density of 2C is stabilized at 101mAh/g and 121.58mAh/g after5cycles respectively. Respectively, it's superior for TiO₂-B/Ag that a large capacity of207.8mAh/g can be achieved again when the current rate was returned to 0.1C even after cycled at different current rates, while the pure TiO₂-B is 144mAh/g, indicating that TiO₂-B/Ag nanocomposite materials for lithium ion battery anode material has a better rate performance.

For further understanding the different kinetics of TiO₂-Band TiO₂-B/Ag hybrid during the electrochemical reaction, the EIS was carried out and the results are shown in Fig.7.Itcan be seen that a semicircle at high frequencies is related to the charge transfer resistance and a short-inclined line in low frequency regions is due to the ion diffusion within the anode [32]. The semicircle diameter of TiO₂-B/Ag is small, which indicates that the composite has higher charge transfer ability and lower electrochemical reaction resistance. This might be contributed to the Ag supported the TiO₂-B nanowires could enhance the electrons conductivity. It also confirms that TiO₂-B/Ag nanocomposites have excellent electrochemical performance, which is consistent with the previous magnifica-

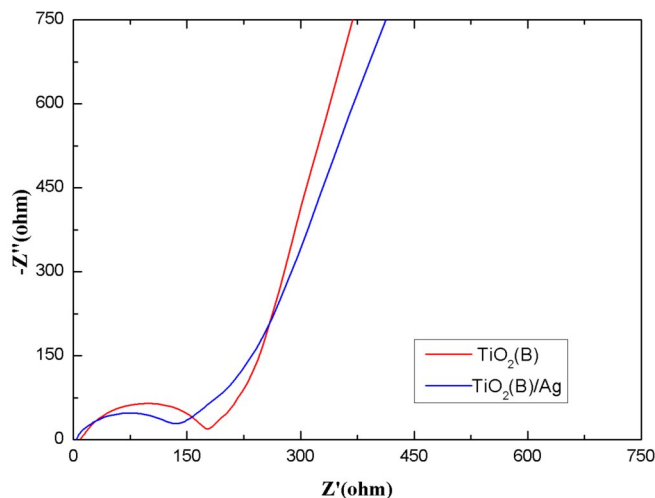


Figure 7. Nyquist plots of EIS results of TiO₂-B/Ag composites and pure TiO₂-B over a frequency range of 100 kHz to 0.01 Hz

tion performance and cyclic performance test. The low slope of the low frequency part reflects the resistance of the ions on the SEI layer, which can be seen from the curves that they have lower impedance.

4. CONCLUSION

In this paper, a facile hydrothermal route is designed for preparing linear TiO₂-B/Ag nanocomposites. As seen from SEM and TEM, the Ag particles are uniformly distributed on the surface of TiO₂-B nanowires, which significantly improve the electrochemical kinetic characteristics of the materials. Besides, according to the electrochemical performance tests, the TiO₂-B/Ag nanocomposites show excellent electrochemical performance. The specific capacity

of TiO₂-B/Ag nanowires reaches 121.58mAh/g at a current density of up to 2C and 172.6mAh/g at a current density of 0.1C. In contrast, the specific capacities of pristine TiO₂-B nanowires materials are 101mAh/g@2C and 144mAh/g@0.1C. Additionally, under charge and discharge cycle test at 0.1C, the initial discharge specific capacity of the TiO₂-B/Ag nanocomposites reaches to 286.369mAh/g, much higher than that of the TiO₂-B nanowires, which is 216.1mAh/g in the first discharge capacity. Also, after 50 cycles, the TiO₂-B/Ag nanocomposites still maintain 126.5mAh/g. These results would shed light on the practical application of Ag compounded materials as high capacity electrode with good cycling stability for next generation LIBs.

5. ACKNOWLEDGEMENTS

This work was supported by the National Natural Science Foundation of China under grant number 51672063 and 51202051 and Science and Technology Program of Zhejiang Province under grant number 2016C31110.

REFERENCES

- [1] C. Liu, F. Li, L.-P. Ma and H.-M. Cheng, *Adv. Mater.*, 22, E28 (2010).
- [2] J. B. Goodenough and K.-S. Park, *J. Am. Chem. Soc.*, 135, 1167 (2013).
- [3] B. Dunn, H. Kamath and J.-M. Tarascon, *Science*, 334, 928 (2011).
- [4] V. Etacheri, R. Marom, R. Elazari, G. Salitra and D. Aurbach, *Energy Environ. Sci.*, 4, 3243 (2011).
- [5] E. Uchaker and G. Cao, *Nano Today*, 9, 499 (2014).
- [6] M. Armand and J. M. Tarascon, *Nature*, 451, 652 (2008).
- [7] Y.-S. Su, Y. Fu, T. Cochell and A. Manthiram, *Nat. Commun.*, 4, 2985 (2013).
- [8] J.-T. Han, Y.-H. Huang and J. B. Goodenough, *Chem. Mater.*, 23, 2027 (2011).
- [9] H. Li, L. Shen, G. Pang, S. Fang, H. Luo, K. Yang and X. Zhang, *Nanoscale*, 7, 619 (2015).
- [10] J. Shu, *Electrochem. Solid-State Lett.*, 11, A238 (2008).
- [11] L. Shen, B. Ding, P. Nie, G. Cao and X. Zhang, *Adv. Energy Mater.*, 3, 1484 (2013).
- [12] M. M. Thackeray, C. Wolverton and E. D. Isaacs, *Energy Environ. Sci.*, 5, 7854 (2012).
- [13] P. G. Bruce, B. Scrosati and J. M. Tarascon, *Angew. Chem., Int. Ed.*, 47, 2930 (2008).
- [14] X. Su, Q. Wu, X. Zhan, J. Wu, S. Wei and Z. Guo, *J. Mater. Sci.*, 47, 2519 (2012).
- [15] Z. Hong and M. Wei, *J. Mater. Chem. A*, 2013, 1, 4403 (2013).
- [16] A. R. Armstrong, G. Armstrong, J. Canales, R. García and P. G. Bruce, *Adv. Mater.*, 17, 862 (2005).
- [17] H. Liu, Z. Bi, X.-G. Sun, R. R. Unocic, M. P. Paranthaman, S. Dai and G. M. Brown, *Adv. Mater.*, 23, 3450 (2011).
- [18] S. Liu, H. Jia, L. Han, J. Wang, P. Gao, D. Xu, J. Yang and S. Che, *Adv. Mater.*, 24, 3201 (2012).
- [19] V. Etacheri, Y. Kuo, A. Van der Ven and B. M. Bartlett, *J. Mater. Chem. A*, 1, 12028 (2013).
- [20] V. Etacheri, J.E. Yourey, B.M. Bartlett, *ACS Nano*, 8, 1491 (2014).
- [21] T. Lan, J. Dou, F. Xie, P. Xiong, M. Wei, *J. Mater. Chem. A*, 3, 10038 (2015).
- [22] Z. Yang, G. Du, Z. Guo, X. Yu, Z. Chen, T. Guo, H. Liu, *J. Mater. Chem.*, 21, 8591 (2011).
- [23] H.C. Tao, L.Z. Fan, X. Yan, X. Qu, *Electrochim. Acta*, 69, 328 (2012).
- [24] Z. Sun, X. Huang, M. Muhler, W. Schuhmann, E. Ventosa, *Chem. Commun.*, 50, 3306 (2014).
- [25] X. Li, Y. Zhang, T. Li, Q. Zhong, H. Li, J. Huang, *J. Power Sources*, 268, 372 (2014).
- [26] X. Yan, Y. Li, M. Li, Y. Jin, F. Du, G. Chen, Y. Wei, *J. Mater. Chem. A*, 3, 4180 (2015).
- [27] M. Zhen, S. Guo, G. Gao, Z. Zhou, L. Liu, *Chem. Commun.*, 51, 507 (2015).
- [28] C. Chen, X. Hu, Z. Wang, X. Xiong, P. Hu, Y. Liu and Y. Huang, *Carbon*, 69, 302 (2014).
- [29] M. Zhen, S. Guo, G. Gao, Z. Zhou and L. Liu, *Chem. Commun.*, (2015).
- [30] T. Beuvier, M. Richard-Plouet, M. Mancini-Le Granvalet, T. Brousse, O. Crosnier and L. Brohan, *Inorg. Chem.*, 49, 8457 (2010).
- [31] Zhang Y, Meng Y, Zhu K, Qiu H, Ju Y, Gao Y, Du F, Zou B, Chen G, Wei Y., *J. Acs Applied Materials & Interfaces* (2016).
- [32] L. Cui, J. Shen, F. Cheng, Z. Tao and J. Chen, *J. Power Sources*, 196, 2195 (2011).